Indisulam synergizes with palbociclib to induce senescence through inhibition of CDK2 kinase activity

Ziva Pogacar[1], Jackie L. Johnson[1], Lenno Krenning[2], Giulia De Conti[1], Cor Lieftink[3], Arno Velds[4], Leyma Wardak[1], Fleur Jochems[1], Kelvin Groot[1], Arnout Schepers[1], Liqin Wang[1], Ji-Ying Song[5], Marieke van de Ven[6], Olaf van Tellingen[7], Rene H. Medema[2], Roderick L. Beijersbergen[1,3], Rene Bernards[1]* and Rodrigo Leite de Oliveira[1,8]*

[1]Division of Molecular Carcinogenesis, Oncode Institute. The Netherlands Cancer Institute, Plesmanlaan 121, 1066 CX Amsterdam, The Netherlands.

[3]The NKI Robotics and Screening Center, The Netherlands Cancer Institute, Plesmanlaan 121, 1066 CX Amsterdam, The Netherlands.

[2]Division of Cell Biology, Oncode Institute, The Netherlands Cancer Institute, Plesmanlaan 121, 1066 CX Amsterdam, The Netherlands.

[4]Genomics core facility, The Netherlands Cancer Institute, Plesmanlaan 121, 1066 CX Amsterdam, The Netherlands.

[5]Division of Animal Pathology, The Netherlands Cancer Institute, Amsterdam, The Netherlands

[6]Mouse Clinic for Cancer and Aging, Netherlands Cancer Institute, Amsterdam, The Netherlands

[7]Division of Pharmacology. The Netherlands Cancer Institute, Plesmanlaan 121, 1066 CX Amsterdam, The Netherlands

[8]Present address: CRISPR Expertise Center, Cancer Center Amsterdam, Amsterdam University Medical Center, De Boelelaan 1117, 1081 HV Amsterdam, The Netherlands

* Correspondence to René Bernards (r.bernards@nki.nl) and Rodrigo Leite de Oliveira (r.ld.oliveira@amsterdamumc.nl).

ABSTRACT

Inducing senescence in cancer cells is emerging as a new therapeutic strategy. In order to find ways to enhance senescence induction by palbociclib, a CDK4/6 inhibitor approved for treatment of metastatic breast cancer, we performed functional genetic screens in palbociclib-resistant cells. Using this approach, we found that loss of *CDK2* results in strong senescence induction in palbociclib-treated cells. Treatment with the CDK2 inhibitor indisulam, which phenocopies genetic CDK2 inactivation, led to sustained senescence induction when combined with palbociclib in various cell lines and lung cancer xenografts. Treating cells with indisulam led to downregulation of cyclin H, which prevented CDK2 activation. Combined treatment with palbociclib and indisulam induced a senescence program and sensitized cells to senolytic therapy. Our data indicate that inhibition of CDK2 through indisulam treatment can enhance senescence induction by CDK4/6 inhibition.

KEYWORDS

CDK4/6 inhibitors, indisulam, senescence, combination treatment

INTRODUCTION

Cellular senescence is a stable cell cycle arrest and can be induced by a variety of stressors, including cancer therapies (referred to as therapy induced senescence [TIS]) [1]. Senescence is characterized by changes in cellular physiology, such as changes of cell morphology, changes in gene expression and metabolism, and secretion of a variety of proteins (collectively referred to as the senescence associated secretory phenotype [SASP])[2]. Induction of senescence as an anti-cancer treatment can be advantageous in the short term because cell proliferation is halted and immune cells are recruited through the SASP. However, in the long term, persistence of senescent cancer cells can lead to chronic inflammation, tumor progression and migration[3]. We postulated that a “one-two punch” approach to cancer therapy, in which a first drug induces senescence and the second drug either targets the senescent cancer cells for death (senolysis) or enhances the efficacy of the immune infiltrate may be an effective anti-cancer strategy[4,5].

Several cancer treatments have been shown to induce senescence, including chemotherapeutics and targeted agents (reviewed in[6]. For instance, targeting CDK4 and 6 with inhibitors (such as palbociclib, ribociclib and abemaciclib) induced senescence in various cancer models[7–11]. CDK4/6 are important kinases in the cell cycle, regulating the transition from G1 to S phase by phosphorylating and partially inactivating the retinoblastoma protein RB. Upon subsequent further phosphorylation of RB by CDK2, RB is functionally fully inactivated, leading to complete de-repression of E2F transcriptional activity and entry into S phase[12]. Since the majority of cancer cells have an intact *RB1* gene and thus depend on CDK4/6 kinase activity for sustained proliferation, CDK4/6 emerged as a potential target for cancer therapy. CDK4/6 inhibitors have been approved for treatment of hormone receptor positive (HR+) and human epidermal growth factor receptor 2 (HER2) negative (HER2-) breast cancer in combination with anti-hormonal therapy[13–15].

Due to the efficacy, safety and tolerability of the CDK4/6 inhibitors in HR+ breast cancer, and multiple nodes of oncogenic signals converging on CDK4/6 in multiple cancer types[16], there has been significant interest in extending their use to other cancer types. Several clinical trials using CDK4/6 inhibitors in various cancer types, such as non-small cell lung cancer, ovarian cancer and triple negative breast cancer were recently completed[17–20]. However, translating the use of CDK4/6 inhibitors to other tumor types has proven to be challenging, due to limited senescence induction and intrinsic resistance[21–23]. Better understanding of the limitations of senescence induction by CDK4/6 inhibitors may help in broadening the clinical utility of this class of cancer therapeutics.

A potential solution is using CDK4/6 inhibitors in a rational combination. For example, combining CDK4/6 inhibitors with PI3K inhibition was effective in multiple preclinical models[24,25]. Furthermore, combining CDK4/6 inhibition with the MEK inhibitor trametinib was shown to increase senescence induction in lung cancer and colorectal cancer cells[26,27].

Indisulam was originally identified as a sulfonamide with anticancer effects. However, after various phase 1 and 2 clinical trials showed a response and stable disease in only 17-36% of patients, development was halted[28–34]. On a molecular level, indisulam was recently identified as being a molecular glue, targeting the splicing factor RBM39 to DCAF15, a component of a ubiquitin ligase complex, leading to degradation of RBM39[35]. Here, we identify an unexpected synergy between indisulam and palbociclib in induction of senescence in multiple cancer types. Moreover, we find that cancer cells made senescent with palbociclib and indisulam are sensitive to the senolytic agent ABT-263.

RESULTS

CDK2 loss is synergistic with palbociclib in inducing senescence in triple negative breast cancer

Palbociclib has only modest cytostatic activity in triple negative breast cancer (TNBC) cell lines (Supplemental Figure 1A). To capture the heterogeneity of TNBC, we chose three independent cell lines as models for kinome-based shRNA synthetic lethality screens to identify genes whose suppression enhances the response to palbociclib. We performed synthetic lethality screens in CAL-51, CAL-120 and HCC1806, all of which are resistant to palbociclib (Figure 1A, Supplemental Figure 1A). Depleted shRNAs were identified by deep sequencing as described previously[36]. When comparing the relative abundance of shRNAs in palbociclib-treated to untreated cells, shRNAs targeting *CDK2* were depleted in all three cell lines (Figure 1B). Furthermore, *CDK2* was the only common hit between all three screening cell lines. To validate this observation, we used individual shRNAs to knock down *CDK2* in the cell lines used for the screens (Supplemental Figure 1B). Even though *CDK2* knockdown had no effect on proliferation, we observed a decrease in proliferation in *CDK2* knockdown cells treated with palbociclib (Supplemental Figure 1C,D). Similarly, CAL-51-*CDK2* knockout cells had no changes in proliferation, but were more sensitive to palbociclib treatment (Figure 1C, D, E).

CDK2 knockout cells treated with palbociclib showed a change in morphology indicative of senescence. To better characterize these cells, we stained them for senescence-associated β-galactosidase (SA-β-gal), an established marker of senescence[37]. We observed an increase in the number of cells positive for SA-β-gal in all three TNBC cell lines when cells lacking *CDK2* were treated with palbociclib (Figure 1F, S1E).

Given that senescent cancer cells can promote inflammation and support metastasis, senolytic therapies are being developed to obliterate the senescent cells[6]. We tested the senolytic compound navitoclax (ABT-263, an inhibitor of BCL-2, BCL-xL and BCL-W) in *CDK2* knockout TNBC cells rendered senescent with palbociclib. After pre-treating sgCDK2 and control cells with palbociclib, only cells lacking CDK2 were killed upon treatment with ABT-263 (Figure 1G).

CDK2 inhibition is synergistic with palbociclib in multiple cancer types

Due to the heterogeneity of TNBC cell lines we hypothesized that the interaction between CDK2 and palbociclib may be a general dependency and could therefore be applied broadly to other cancer types. To address this, we tested an additional TNBC cell line (SUM159) as well as lung cancer cell lines A549 and H2122 and colorectal cancer cell lines DLD-1 and RKO. We knocked out *CDK2* (Figure 2A, E, S2A, C, E) and observed an increased sensitivity to palbociclib in cells harboring sgCDK2 compared to control cells (Figure 2B, C, F, G, S2B, D, F). Furthermore, cells harboring sgCDK2 treated with palbociclib showed an increased number of SA-β-gal positive cells in SUM159 and A549 (Figure 2D, H) and the enlarged size and flat morphological features of cellular senescence. Unequivocal identification of senescence in cancer cells can be difficult due to the lack of gold-standard markers of the senescent state. Previous studies have identified gene signatures associated with senescence[2,38] or list of genes differentially expressed in senescence[39,40]. We therefore used transcriptome analyses to further characterize these cells. We observed that A549 cells showed enrichment in four out of five tested senescence signatures in RNA-seq experiments when comparing treated and untreated sgCDK2 cells (Figure 2I). This shows that senescence induction upon *CDK2* loss and CDK4/6 inhibition has little context-dependency.

Indisulam phenocopies CDK2 loss and induces senescence in combination with palbociclib

Even though the interaction between *CDK2* loss and palbociclib induces senescence in a broad panel of cell lines, the lack of a selective CDK2 inhibitor complicates further development of this concept. While a variety of compounds targeting CDK2 are available, they tend to be non-specific and also target other CDKs, such as CDK1/5/7/9 (reviewed in [41]which diminishes their utility. Furthermore, the off-target effects of these compounds often lead to toxicity and prevent their use in combination therapies. In search of a CDK2

inhibitor we came across indisulam, a sulfonamide that was described as an indirect CDK2 inhibitor[42]. When we treated the cells with the combination of palbociclib and indisulam we observed a decrease in proliferation in all tested cell lines (Figure 3A, B, S3A, B). Furthermore, treatment with indisulam and palbociclib showed an increase in the number of cells positive for SA-β-gal (Figure 3C, S3C). Both SUM159 and A549, as well as CAL-51 senescent cells induced by palbociclib and indisulam were sensitive to ABT-263 (Figure 3D, S3D).

We then set out to further characterize the senescence phenotype by testing four different senescence markers by Western blot. We observed a decrease in phosphorylated RB and increase in p21 in both cell lines. There was also an increase in γH2AX, although less apparent in A549. Furthermore, there was an increase in p16INK4A in SUM159. Since A549 cells are p16 null, we examined an additional marker Lamin B1, which was reduced upon the combination treatment. We observed a reduction in CDK2 protein levels in palbociclib treated samples, however CDK2 was not further reduced upon the combination treatment samples (Figure 3E).

Next, we treated A549 and SUM159 cells with indisulam, palbociclib and the combination, and performed RNA-sequencing. We observed enrichment in senescence signatures when comparing the combination-treated cells to single drugs or untreated conditions (Figure 3F). Additionally, we tested the recently developed PF-0687360 compound, which is described to inhibit CDK2/4/6[43,44]. Treatment with PF-0687360 led to an increase of SA-β-gal positive cells in SUM159 and A549 (Figure S3E) as well as enrichment in senescence signatures (Figure S3F), further validating inhibition of CDK2 with CDK4/6 as a senescence inducing combination.

Combination of indisulam and palbociclib impairs tumor growth *in vivo*

To extend the findings to an *in vivo* model, we tested if *CDK2* loss leads to growth arrest when combined with palbociclib treatment in mice xenografts. We generated *CDK2* KO clones in A549 and CAL-51 cells and then engrafted A549 subcutaneously and CAL-51 orthotopically in NMRI nude mice. However, *CDK*2 seems to be essential for growth *in vivo* as the growth of *CDK2* knock-out tumors was severely impaired, making genetic validation technically not feasible (Figure S4A, B). We then proceeded to test the combination of palbociclib and indisulam *in vivo*. Firstly, we performed a PK/PD experiment and determined that both drugs were stable in plasma (Figure S4C, D). Next, we engrafted A549 cells subcutaneously and treated the mice with vehicle, palbociclib, indisulam or the combination. We observed a reduction in tumor growth in animals treated with the drug combination compared to the single treatments (Figure 4A). Furthermore, immunohistochemical analysis showed decrease of the proliferation marker Ki67 and increase of the CDK inhibitor p21 in tumors treated with the drug combination, compared to single treatments or control groups (Figure 4B, C). We conclude that the combination of indisulam and palbociclib is well tolerated in vivo and leads to impaired tumor growth and reduced proliferation.

Indisulam prevents activation of CDK2 leading to cell cycle arrest when combined with palbociclib

To better understand the effects of indisulam on CDK2 we first performed an *in vitro* kinase activity assay. In short, we added indisulam to different cyclin/CDK complexes in vitro and measured the kinase activity as previously described[45]. We did not observe a direct and specific inhibition of CDK2 by indisulam, which was in line with previous reports on indisulam being an indirect CDK2 inhibitor (Figure S5A). Recently, indisulam has been characterized as a molecular degrader, bringing together a splicing factor RBM39 with DCAF15 substrate receptor of CUL4a/b ubiquitin ligase complex[35]. This leads to ubiquitination and proteasomal degradation of RBM39, leading to accumulation of splicing errors. We therefore asked whether RBM39 degradation plays a role in the senescence induction by palbociclib and indisulam. Indeed, we observed a degradation of RBM39 in cells treated with indisulam

or the combination with palbociclib (Figure 5A). To understand if the combination effect of palbociclib and indisulam is dependent on RBM39 we used shRNAs to knock down RBM39. We observed that cells with reduced RBM39 expression and treated with palbociclib showed a reduction in growth (Figure 5B, C) and became positive for SA-β-gal staining (Figure 5D). This suggests that the senescence induction upon indisulam and palbociclib treatment is mediated through RBM39 degradation.

To characterize splicing errors downstream of RBM39 degradation we treated A549 and SUM159 cells with indisulam, palbociclib or the combination and collected an RNA-seq data. Upon quantifying the splicing errors (see methods) we detected an increase of splicing errors in indisulam-treated and combination-treated cells with skipped exons being the most common splicing error class detected (Figure 5E).

To elucidate how indisulam-induced splicing errors affect CDK2 activity, we made use of a CDK2 reporter construct that changes its subcellular localization depending on CDK2 activity[46]. Cells with low CDK2 activity show fluorescence in the nucleus and cells with active CDK2 show fluorescence in the cytoplasm. Upon 24 hours treatment with a matrix of increasing concentrations of indisulam, palbociclib and the combination we imaged fixed cells and determined the nuclear and cytoplasmic fluorescence signal, indicative of CDK2 activity. We observed a decrease of CDK2 activity in cells treated with the combination of indisulam and palbociclib (Figure 5F). To exclude a potential confounding effect of cell cycle arrest leading to reduced CDK2 activity in the combination treatment, we performed a FACS-based experiment, where we did not observe cell cycle differences between the single treatments and the combination after 24h (Figure 5G). This indicates that CDK2 inactivation happens upstream of cell cycle arrest.

To investigate the dynamic of CDK2 inactivation upon treatment we performed a live imaging experiment using CDK2 reporter cells. We included a positive control, a CDK1/2 inhibitor SNS-032. After beginning the imaging, the drugs were added and cells were followed

through their next cell cycle. We first followed the cells that showed the fluorescence signal in the cytoplasm, indicative of active CDK2. We observed inactivation of CDK2 when we added SNS-032, but not the other drugs. Next, we followed the cells that showed fluorescence in the nucleus, and therefore had low activity of CDK2. We observed that treatments with SNS-032 and palbociclib prevented CDK2 activation, as expected. Remarkably, treatment with indisulam prevented CDK2 activation as well (Figure 5H).

When examining the effects of the combination treatment on the cell cycle proteins we observed a stronger reduction in phosphorylated RB in the combination treated cells (Figure 5I). While levels of total CDK2 were only slightly reduced, the difference is likely in the levels of active CDK2. Additionally, Cyclin E levels were increased upon palbociclib treatment, which can be explained by reduced CDK2 activity regulating cyclin E levels[47,48]. We also observed a decrease in Cyclin H, a member of the CDK activating complex (CAK). CAK phosphorylates and activates CDK2 and we hypothesized that indisulam-induced downregulation of Cyclin H could lead to CDK2 inactivation. To this end, we tested the expression levels of *CCNH* upon treatment with indisulam using qPCR and observed a downregulation in both A549 and SUM159 cells (Figure 5J). Additionally, cells with knockdown of RBM39 also showed a reduction in *CCNH* (Figure 5K). This might indicate that indisulam-induced *CCNH* downregulation prevents CDK2 activation through the CAK complex. We then analyzed the RNA-seq data generated in Figure 5E by performing a kinase enrichment analysis[49]. Genes associated with CDK1 and CDK2 were over-represented in the list of differentially expressed genes in A549 and SUM159 cells treated with indisulam (Figure S5D). This further indicates that treatment with indisulam reduces the activity of CDK2. To confirm the effect of indisulam on CDK2, we overexpressed CDK2 in A549 cells using both transient transfection and stable integration of lentiviral vectors (Figure 5L, M, S5B, C). We observed an increase in proliferation rescuing the senescence induction in cells that overexpressed CDK2 compared to control cells. Senescence induction was not fully rescued by CDK2 overexpression, which is in line with the observation that the activity

and not only abundance of CDK2 determine senescence induction. Taken together, indisulam downregulates *CCNH*, which prevents CDK2 activation and leads to senescence induction when combined with palbociclib.

DISCUSSION

Since proliferation of cancer cells depends heavily on the core components of the cell cycle machinery, inhibitors of CDKs could have significant anticancer activity in many tumor types. However, translating the success of CDK4/6 inhibitors from HR+ breast cancer to other cancer types has been hampered by intrinsic resistance[23,50]. Here we identify a treatment strategy that exploits the synergy between CDK2 loss (i.e., indisulam treatment) and palbociclib treatment in induction of senescence in a diverse panel of cell lines.

Genetic screens are a powerful tool to identify genetic dependencies in an unbiased manner[51]. Here, we identified *CDK2* loss as an enhancer of the palbociclib effect using genetic screens in three TNBC cell lines. We further validated this interaction in a diverse panel of cell lines, demonstrating that this synergy shows little context dependency. The interaction between *CDK2* loss and CDK4/6 inhibition is not surprising, as CDK2 acts downstream of CDK4/6 in the cell cycle progression. Furthermore, the majority of clinically relevant resistance mechanisms to CDK4/6 inhibition, such as loss of RB and overexpression of *CCNE[20]*, could be circumvented by CDK2 inhibition. As such, *CDK2* depletion was previously shown to re-sensitize both CDK4/6 inhibitor sensitive and resistant cells[22,24,43,52,53].

Unfortunately, the lack of a specific CDK2 inhibitor has until now prevented exploiting the synergy between CDK2 inhibition and CDK4/6 inhibition. In spite of this, multiple targeting strategies were previously described to increase sensitivity to CDK4/6 inhibition, such as using a multi CDK inhibitor roscovitine[24], knock-in of analog-sensitive CDK2[22] and use of

296 triple CDK2/4/6 inhibitor PF-06873600[43,44]. Unfortunately, the use of roscovitine in the
297 clinic is hindered by off-target effects and toxicity, and analog-sensitive CDK2 lacks
298 translational potential. Even though PF-06873600 is in clinical development (phase 1 clinical
299 trial ongoing: NCT03519178), the compound also inhibits CDK1, which might lead to toxicity
300 as seen with other multi-CDK inhibitors[43]. Interestingly, comparing palbociclib to two other
301 CDK4/6 inhibitors abemaciclib and ribociclib shows that abemaciclib is more effective
302 compared to palbociclib and ribociclib, possibly due to the notion that it also targets
303 CDK2[45]. However, both intrinsic and acquired resistance are still an issue, indicating a
304 need for a different therapeutic strategy. We propose using the indirect CDK2 inhibitor
305 indisulam, which has previously shown a favorable toxicity profile in the clinic. We
306 demonstrate that combination of palbociclib and indisulam induces senescence in a diverse
307 cell line panel, which points to a broad applicability across tumor types. Additionally, our
308 preliminary data indicate that the combination can be effective in vivo.
309
310 Even though indisulam was described as an indirect CDK2 inhibitor, later studies revealed
311 that it targeted a splicing factor—RBM39—for degradation. Interestingly, we observed an
312 effect of indisulam on CDK2 activity only in cells where CDK2 is initially inactive, indicating
313 that indisulam prevents CDK2 activation. Regulation of CDK2 activity is based on its
314 interaction with cyclins, removal of inhibitory phosphorylation by CDC25 and activating
315 phosphorylation by the CDK Activating Kinase (CAK) complex. We observed that cyclin H,
316 which is a part of the CAK complex, is downregulated upon indisulam treatment in an
317 RBM39 dependent manner. As we observed no splicing errors in *CCNH* transcripts or other
318 CDK2 regulators, it is still unclear how reduction of RBM39 leads to *CCNH* downregulation.
319 As *CCNH* is an essential gene, loss of function genetic experiments are technically
320 challenging to perform. Additionally, other CDKs might be involved in senescence induction
321 through indisulam since CAK regulates CDK1,4 and 6 in addition to CDK2. Furthermore, as
322 activity and not amount of CDK2 seems to play a role in indisulam sensitivity,

overexpression of CDK2 is at best expected to partially rescue the senescence induction, which is indeed what we observed here.

Combining palbociclib with indisulam might be a potential treatment strategy for cell types that are intrinsically resistant to palbociclib. In addition, acquired resistance to palbociclib has been shown to be reversed by depleting CDK2. For example, loss of RB leads to resistance to palbociclib and the combination of palbociclib with a MEK inhibition[26]. However, RB deficient cells are still sensitive to knockdown of CDK2[53]. It is therefore likely that the combination of palbociclib and indisulam would still be effective in palbociclib resistant cells, although the mechanism of senescence induction in RB deficient cells is not yet well understood. Furthermore, recent reports on Cyclin D regulation described *AMBRA1* loss as a resistance mechanism to CDK4/6 inhibition,[54] but as those cells still depend on CDK2 activity, combination with indisulam could still be effective. Senescence induction is increasingly in focus as a potential cancer therapeutic strategy, supported by the findings that senolytic compounds can be effective in eradicating senescent cancer cells[6]. Here, we have shown that senescence induction by palbociclib and indisulam sensitizes the cells to the established senolytic drug navitoclax. Finally, senescent cells attract immune cells, and together with the notion that indisulam induced splicing errors could lead to generation of neoantigens, the combination of senescence induction and immunotherapy might be a potential future treatment strategy[26,55].

ACKNOWLEDGEMENTS

We would like to thank Artur Burylo, Natalie Proost, Jordi van Iersel and Marcio Sousa for help with experiments and Katrien Berns for critical discussion on screening techniques. We also thank the NKI Bioimaging facility, Genomics core facility and pre-Clinical Intervention Unit for their technical support. This work was supported by grants from the European Research Council (ERC) to R.B. and the Dutch Cancer Society through the Oncode Institute.

AUTHOR CONTRIBUTIONS

Conceptualization, Z.P, J.L.J, R.B and R.L.O.; Methodology, L.K.; Software C.L., A.V. and K.G.; Validation, Z.P. and R.L.O.; Formal analysis, Z.P., G.D.C., C.L., A.V., K.G., Le. W., F.J., J.Y.S. and R.L.O.; Investigation, Z.P., J.L.J., L.K., G.D.C., Le.W., F.J., K.G., A.S., Li.W., J.Y.S. and R.L.O.; Data curation, C.L. and A.V.; Writing - Original Draft, Z.P., R.B. and R.L.O.; Writing - Review and Editing, J.L.J., F.J., A.S., Li.W., O.vT. and R.L.B.; Visualization, Z.P., L.K., G.D.C., C.L., A.V., Le.W., F.J., K.G. and R.L.O.; Supervision, M.vdV., O.vT., R.H.M., R.L.B. and R.B.; Funding Acquisition, R.H.M and R.B.

DECLARATION OF INTEREST

R.B is the founder of the company Oncosence (https://www.oncosence.com), which aims to develop senescence-inducing and senolytic compounds to treat cancer.

LEGENDS

Figure 1: CKD2 loss is synergistic with palbociclib in induction of senescence in triple negative breast cancer

A Volcano plot of hit selection. shRNA counts of CAL-51, CAL-120 and HCC1806 were compared between palbociclib treated and untreated conditions. Each dot represents an individual shRNA. Y axis shows the false discovery rate (FDR) and X axis shows fold change between conditions. The cutoffs of 0.1 FDR and -1 log2 fold change are represented by the dashed lines. Red dots indicate shRNAs targeting CDK2. Hits were selected as genes that were represented with at least 2 independent shRNAs.

B Venn diagram shows overlap of hits between CAL-51, CAL-120 and HCC-1806. Hits were selected as genes that were represented with at least 2 independent shRNAs.

C-F Screen validation: CDK2 was knocked out with two independent sgRNAs in CAL-51 cells.

C Western blot analysis of CDK2 levels in CAL-51 sgCDK2 and control cells. Tubulin was used as loading control (n=2).

D Long term colony formation assay of CAL-51. Wild-type, control and sgCDK2 cells were treated with indicated doses of palbociclib for 10 days (n=3).

E Proliferation assay of CAL-51. Cells were treated with 0.5 µM of palbociclib or DMSO. Mean of three technical replicates (n=2) is shown and error bars indicate standard deviation. The end point confluency of all conditions were analysed using two-way ANOVA with Šidák's post-hoc test (** $p< 0.01$ **** $p< 0.0001$).

F SA-β-gal staining in CAL-51 cells treated for 10 days with 0.5 µM of palbociclib. Scale bar indicates 100 µm (n=2).

G Proliferation assay of CTRL or CAL-51 sgCDK2 cells treated with senolytic drug ABT-263. Cells were pre-treated with 2 µM of palbociclib for 10 days to induce senescence, then seeded in high density (100% confluence) and treated with palbociclib or a combination of palbociclib and 5 µM ABT-263. Proliferating cells, which were not pre-treated, were seeded at low density and treated with DMSO or ABT-263. Mean of three technical replicates is shown and error bars indicate standard deviation (n=2).

Figure 2: CDK2 inhibition is synergistic with palbociclib in multiple cancer types

A-D CDK2 was knocked out in SUM159 cells using two independent sgRNAs.

A Western blot analysis of SUM159 sgCDK2 cells and control cells. Tubulin was used as a loading control (n=2).

B Long term colony formation assay of SUM159 sgCDK2 and control cells with palbociclib was performed for 8 days (n=2).

C Proliferation assay of SUM159 sgCDK2 and control cells treated with 0.25 µM of palbociclib. Mean of three technical replicates (n=2) is shown and error bars indicate standard deviation. The end point confluency of all conditions were analysed using two-way ANOVA with Šidák's post-hoc test (**** $p< 0.0001$).

D SA-β-gal staining in SUM159 sgCDK2 and control cells treated with 0.25 µM of palbociclib for 8 days. Scale bar indicates 100 µm (n=2).

E-H CDK2 was knocked out in A549 and two single cell clones were selected.

E Western blot analysis of A549 sgCDK2 cells and control cells. Tubulin was used as a loading control (n=2).

F Long term colony formation assay of A549 sgCDK2 and control cells with palbociclib was performed for 10 days (n=2).

G Proliferation assay of A549 sgCDK2 and control cells treated with 0.5 µM of palbociclib. Mean of three technical replicates (n=2) is shown and error bars indicate standard deviation. The end point confluency of all conditions were analysed using two-way ANOVA with Šidák's post-hoc test (**** p< 0.0001).

H SA-β-gal staining in A549 sgCDK2 and control cells treated with 0.5 µM of palbociclib for 10 days. Scale bar indicates 100 µm (n=2).

I GSEA of previously published senescence gene sets comparing A549 sgCDK2 cells treated with 2 µM palbociclib for 10 days with untreated cells. Normalized enrichment score (NES) and p-values of enrichment score are shown. The experiment was performed in duplicates.

Figure 3: Indisulam phenocopies CDK2 loss and induces senescence in combination with palbociclib

A Long term colony formation assay of SUM159 and A549 cells treated with palbociclib, indisulam and the combination for 10 days (n=3).

B Proliferation assay of SUM159 and A549 cells treated with palbociclib, indisulam and the combination. SUM159 cells were treated with 0.5 µM of palbociclib and 2 µM indisulam and A549 with 2 µM palbociclib and 0.5 µM indisulam. Mean of three technical replicates (n=2) is

shown and error bars indicate standard deviation. The end point confluency of all conditions were analysed using one-way ANOVA with Dunnett's post-hoc test (**** p< 0.0001).

C SA-β-gal staining in SUM159 and A549 cells treated with palbociclib, indisulam and combination. SUM159 were treated with 0.5 µM of palbociclib and 2 µM indisulam and A549 with 2 µM palbociclib and 0.5 µM indisulam for 10 days. Scale bar indicates 100 µm (n=3).

D Long term colony formation assay of SUM159 and A549 cells pre-treated with 0.5 µM of palbociclib plus 2 µM of indisulam for SUM159 and 2 µM of palbociclib plus 0.5 µM of indisulam for A549 for 2 weeks. Senescent and parental cells were then treated with 0.5 µM and 2 µM of ABT-263 for 1 week (n=2).

E Western blot analysis of SUM159 and A549 cells treated with palbociclib, indisulam and combination. SUM159 were treated with 0.5 µM of palbociclib and 2 µM indisulam and A549 with 2 µM palbociclib and 0.5 µM indisulam for 10 days. HSP90 and vinculin were used as a loading control (n=2).

F GSEA of previously published senescence gene sets comparing A549 and SUM159 cells treated with palbociclib, indisulam or the combination. SUM159 were treated with 0.5 µM of palbociclib and 2 µM indisulam and A549 with 2 µM palbociclib and 0.5 µM indisulam for 10 days. Comparisons of normalized enrichment scores of combination with untreated, and combination with single drugs is shown. Numbers indicate p-value (*p<0.05; **p<0.01; ***p<0.001).

Figure 4: Combination of indisulam and palbociclib impairs tumor growth *in vivo*

A Tumor growth of A549 xenografts in NMRI nude mice. Upon tumors reaching 200 mm^3 the mice were randomly assigned to treatment with vehicle, indisulam, palbociclib or combination. Palbociclib was administered by oral gavage daily at 100 mg/kg and indisulam by intraperitoneal injection three times per week at 5 mg/kg. Every group consisted of 8-12 mice. Error bars indicate SEM. Tumor volumes of palbociclib and combination treated mice at end point were analysed using unpaired t-test (*p<0.05).

B Quantification of IHC staining for Ki67 and p21 of A549 tumor xenografts (n= 8-12). Positive area of the tumor was quantified in tumors treated with vehicle, palbociclib, indisulam or combination. One-way ANOVA was performed with Dunnett's post-hoc test (*p<0.05; ***p<0.001; ****p<0.0001). For the Ki67 staining, combination is compared to vehicle or single treatments.

C Representative images from (B) of IHC staining for Ki67 and p21 of A549 tumor xenografts treated with vehicle, palbociclib, indisulam or combination. Images were taken at 20x magnification and the scale bar indicates 50 µm.

Figure 5: Indisulam prevents activation of CDK2 leading to cell cycle arrest when combined with palbociclib

A Western blot analysis of RBM39 in SUM159 and A549 cells treated with palbociclib, indisulam or combination. SUM159 were treated with 0.5 µM of palbociclib and 2 µM indisulam and A549 with 2 µM palbociclib and 0.5 µM indisulam for 12 days. Vinculin was used as a loading control (n=3).

B-D RBM39 was knocked-down in SUM159 cells with two independent shRNAs.

B qPCR analysis of RBM39 normalized to housekeeping gene RPL13 in SUM159. Mean of three technical replicates is shown and error bars indicate standard deviation.

C Proliferation assay was performed in RBM39 knock-down and control SUM159 using 0.25 µM of palbociclib. Mean of three technical replicates is shown and error bars indicate standard deviation. The end point confluency of all conditions were analysed using two-way ANOVA with Šidák's post-hoc test (**** p< 0.0001).

D SA-β-gal staining in RBM39 knock-down and control SUM159 cells treated with 0.125 µM of palbociclib for 10 days. Scale bar indicates 100 µm (n=2).

E Quantification of splicing errors in RNA-sequencing data in A549 and SUM159 cells treated for 16h with 2 µM palbociclib, 3 µM indisulam and the combination, in technical duplicates. Bars represent counts compared to untreated samples.

F A549 cells expressing a CDK2 reporter DHB-iRFP and H2B-GFP were treated with a matrix of different concentrations of palbociclib (2-5 µM) and indisulam (2-40 µM). After 24h, CDK2 reporter localization and nuclei were imaged by spinning disk microscopy, and the nucleo/cytoplasmic distribution of the CDK2 reporter was analyzed using ImageJ. Matrix shows the average CDK2 reporter ratio (n=2).

G Flow cytometry analysis of A549 cells treated with 5 µM of palbociclib, 40 µM of indisulam or combination for 24h. Mean of three technical replicates is shown and error bars represent standard deviation. Unpaired t-test was performed (*p<0.05; **p<0.01) (n=2).

H A549 cells expressing CDK2 reporter DHB-iRFP and H2B-GFP were treated with 10 µM of SNS-032, 40 µM of indisulam or 5 µM palbociclib and immediately imaged for 24h. CDK2 activity was quantified in cells with initial high CDK2 activity (left plot) and cells with initial low CDK2 activity (right plot). At least 10 cells per condition were quantified and results show the mean of two biological replicates. Error bars indicate standard deviation (n=2).

I Western blot analysis of A549 and SUM159 cells treated with 2 µM palbociclib, 5 µM indisulam and the combination for either 24 or 48 hours. HSP90 was used as a loading control (n=3).

J qPCR analysis of A549 and SUM159 cells treated with 3 µM of indisulam for 24h. CCNH expression was normalized to the housekeeping gene RPL13. Mean of three technical replicates is shown and error bars indicate standard deviation.

K qPCR analysis of SUM159 cells harbouring shRBM39 or control cells for CCNH (as in B). Expression was normalised to the housekeeping gene RPL13. Mean of three technical replicates is shown and error bars indicate standard deviation.

L qPCR analysis of CDK2 overexpressing A549 cells compared to GFP control cells. Expression was normalized to the housekeeping gene RPL13. Mean of three technical replicates is shown and error bars indicate standard deviation.

M Long term colony formation assay of CDK2 and GFP overexpressing A549 cells treated with 0.5 µM palbociclib, 0.5 µM indisulam and the combination for 10 days.

SUPPLEMENTAL FIGURE LEGENDS

Supplemental Figure 1

A Schematic outline of dropout screens. Triple negative breast cancer cell lines CAL-51, CAL-120 and HCC1806 were infected with a shRNA library targeting kinome and cultured in presence or absence of palbociclib. After 8 - 10 population doublings, shRNA sequences were amplified and quantified using next generation sequencing.

B-E CDK2 was knocked down in CAL-51, CAL-120 and HCC1806 using two independent shRNAs.

B qPCR analysis of CDK2 normalized against expression of housekeeping gene RPL13. Mean of three technical replicates is shown and error bars indicate standard deviation.

C Long term colony formation assay with palbociclib was performed for 10 days (n=3).

D Proliferation assay was performed using 0.5 µM of palbociclib for CAL-51 and CAL-120 and 2 µM for HCC1806. Mean of three technical replicates (n=2) is shown and error bars indicate standard deviation. The end point confluency of all conditions were analysed using two-way ANOVA with Šidák's post-hoc test (** $p < 0.01$, **** $p < 0.0001$)

E SA-β-gal staining in CAL-51, CAL-120 and HCC1806 CDK2 KD and control cells treated for 10 days with 0.5 µM of palbociclib. Scale bar indicates 100 µm (n=2).

Supplemental Figure 2

A-C CDK2 was knocked out in DLD-1, RKO and H2122 cells using two independent sgRNAs.

A Western blot analysis of CDK2 knock-out DLD-1, RKO and H2122 cells and control cells. Tubulin was used as a loading control. An arrow depicts the CDK2 band in H2122 (n=2).

B Long term colony formation assay of DLD-1, RKO and H2122 sgCDK2 and control cells with palbociclib was performed for 10 days (n=2).

C Long term colony formation assay of control and SUM159 sgCDK2 cells pre-treated with 2 µM palbociclib for 2 weeks, and then treated with 0.5 µM ABT-263 for 1 week (n=2).

Supplemental Figure 3

A Long term colony formation assay of CAL-51, DLD-1, RKO and H2122 cell lines treated with palbociclib, indisulam and the combination for 10 days (n=2).

B Proliferation assay of CAL-51, DLD-1, RKO and H2122 cell lines treated with palbociclib, indisulam and the combination. CAL-51 were treated with 1 µM of palbociclib and 1 µM indisulam, DLD-1 with 0.5 µM of palbociclib and 1 µM indisulam, RKO with 2 µM of palbociclib and 1 µM indisulam and H2122 with 1 µM palbociclib and 0.5 µM indisulam. Mean of three technical replicates (n=2) is shown and error bars indicate standard deviation. The end point confluency of all conditions were analysed using one-way ANOVA with Dunnett's post-hoc test.**** $p < 0.0001$

C SA-β-gal staining in CAL-51, DLD-1, RKO and H2122 cell lines treated with palbociclib, indisulam and the combination using the same doses as in B. Scale bar indicates 100 µm (n=2).

D Long term colony formation assay of CAL-51 cells pre-treated with 1 µM of palbociclib and 1 µM of indisulam for 2 weeks. Senescent and parental cells were then treated with 0.5 µM and 2 µM of ABT-263 for 1 week (n=2).

E SA-β-gal staining in A549 and SUM159 cell lines treated with 0.5 µM PF-06873600 for one week (n=2).

F GSEA of previously published senescence gene sets comparing A549 and SUM159 cells treated with 0.5 µM PF-06873600 for one week with untreated cells. Normalized enrichment score (NES) and p-values of enrichment score are shown. The experiment was performed in duplicates.

Supplemental Figure 4

A Tumor growth of CAL-51CDK2 single cell knock-out clone and control xenografts in mice. One million cells were injected orthotopically in the 4th right mammary fat pad of female NMRI nude mice, 5-6 mice per group.

B Tumor growth of two A549 CDK2 single cell knock-out clones and control xenografts in mice. One million cells were injected subcutaneously in the right flank of NMRI nude mice, 5-6 mice per group.

C, D Pharmacokinetic studies of palbociclib and indisulam in A549-tumor bearing mice. A549 cells were injected subcutaneously in NMRI nude mice. After tumour establishment (~200 mm3), mice were treated with palbociclib, indisulam or combination. Blood was collected 2, 4, 8 and 24h after drug treatment from 6 male and 6 female mice. The drug concentrations in the blood were determined by mass spectrometry.

C Palbociclib blood concentration is displayed from every mouse that received the single drug treatment (left) and the combination with indisulam (right).

D indisulam blood concentration is displayed from every mouse that received the single drug treatment (left) and the combination with palbociclib (right).

Supplemental Figure 5

A In vitro kinase inhibition assay of indisulam for CDK/cyclin complexes. IC50 values are shown in triplicates with error bars indicating standard deviation.

B qPCR analysis of A549 cells transfected with CMV-CDK2 and CMV-GFP vectors. Expression was normalized to the housekeeping gene RPL13. Mean of three technical replicates is shown and error bars indicate standard deviation.

C Long term colony formation assay of A549 cells transfected with CMV-CDK2 and CMV-GFP vectors treated with 0.5 µM palbociclib, 0.5 µM indisulam and the combination for 10 days.

D Kinase enrichment analysis (KEA) on RNA-seq data in A549 and SUM159 cells treated with 3 µM indisulam for 16h compared to untreated. Filtered for adjusted p-value <0.05. CDK1 and CDK2 are highlighted.

Materials availability

Plasmid generated in this study is available from the corresponding authors upon request.

Data and Code availability

Raw RNA-sequencing data will be available in GEO upon acceptance of the manuscript.

METHODS

Cell lines

TNBC cell line CAL-51 was grown in DMEM (Gibco) supplemented with 20% fetal bovine serum (FBS, Serana), 1% penicillin-streptomycin (P/S, Gibco) and 2mM L-glutamine (Gibco). TNBC cell line CAL-120 was grown in DMEM supplemented with 10% FBS, 1% P/S and 2 mM L-glutamine. TNBC cell line HCC1806, lung cancer cell lines A549 and H2122, colon cancer cell lines DLD-1 and RKO were grown in RPMI (Gibco) supplemented with 10% FBS, 1% P/S and 2 mM L-glutamine. TNBC cell line SUM159 was grown in DMEM/F12 (Gibco) supplemented with 10% FBS, 1% P/S, 5 µg/ml insulin (Sigma-Aldrich) and 1µg/ml hydrocortisone (Sigma-Aldrich).

HCC1806, A549, RKO, H2122 and DLD-1 were purchased from ATCC. SUM159 was a gift from Metello Innocenti (NKI, Amsterdam). CAL-51 and CAL-120 were obtained from DSMZ. All cell lines were regularly tested for mycoplasma contamination using a PCR assay and STR profiled (Eurofins).

Compounds and antibodies

Palbociclib, indisulam and ABT-263 were purchased from MedKoo (Cat:#123215, #201540 and #201970). PF-06873600 was purchased from Selleck chem. Antibodies against CDK2 and tubulin were purchased from Abcam. Antibodies against vinculin and p-H2AX S139 were purchased from Sigma Aldrich. Antibodies against p-RB S780, p-RB S795, RB (9309-4H1), Lamin B1, Cyclin H and Cyclin E were purchased from Cell Signalling Technology. Antibodies against HSP90 and p21 were purchased from Santa Cruz Biotechnology. Antibody against RBM39 was purchased from Atlas Antibodies. Antibody against p16 was purchased from Proteintech.

628

629 **Kinome dropout shRNA screens**

630 TNBC cell lines CAL-51, CAL-120 and HCC1806 were screened using a kinome shRNA
631 library targeting 518 human kinases and 17 kinase-related genes. The kinome library was
632 assembled from the RNAi Consortium (TRCHs 1.5 and 2.0) shRNA collection and included
633 243 hairpins targeting essential and 272 targeting non-essential genes. Upon generating
634 lentiviral shRNA vectors, CAL-51, CAL-120 and HCC1806 cells were infected using a low
635 infection efficiency of <30%, reference sample t=0 was collected and cells were then
636 cultured in the presence or absence of palbociclib (0.4 µM for CAL-51, 1 µM for CAL-120
637 and 0.2 µM for HCC1806), while maintaining 1000x coverage of the library. shRNA
638 sequences were then recovered by PCR from genomic DNA, and the abundance was
639 quantified by deep sequencing. The analysis was performed using DESeq[56]. Hit selection
640 was done in two steps: initially the hits were selected based on the comparison of treated to
641 untreated arm with the criteria of at least two shRNAs per gene with log2 fold change <-1,
642 FDR <0.1 and baseMeanA > 100 and no hit shRNAs in the opposite direction. To exclude
643 the shRNAs that are increased in the untreated condition, instead of decreased in treated
644 compared to reference t=0 sample, we performed an additional selection step in which
645 sgRNA should have log2 fold change < -1 in treated condition compared to reference t=0
646 condition. Hits that overlapped between the three cell lines were prioritized for validation.

647

648 **Plasmids**

649 The lentiviral shRNA vectors were selected from the arrayed TRC human genome-wide
650 shRNA collection in pLKO backbone. shRNA targeting CDK2 #1:
651 CTATGCCTGATTACAAGCCAA, shRNA targeting CDK2 #2:
652 GCCCTCTGAACTTGCCTTAAA, shRNA targeting RBM39 #1:
653 GCCGTGAAAGAAAGCGAAGTA, shRNA targeting RBM39 #2:
654 GCTGGACCTATGAGGCTTTAT. Single gRNAs were cloned into LentiCRISPR 2.1 plasmid
655 [57] by BsmBI (New England BioLabs) digestion and Gibson Assembly (New England

BioLabs); control sgRNA: ACGGAGGCTAAGCGTCGCAA, sgRNA targeting CDK2 #1: GTTCGTACTTACACCCATGG, sgRNA targeting CDK2 #2: CATGGGTGTAAGTACGAACG. For overexpression experiments pLX304-Blast-V5 were used, with either GFP or CDK2 (ID ccsbBroad304_00276). Additionally, pCMV-GFP (Addgene #11153) and pCMV-CDK2[58] were used to transiently transfect the target cells.

Lentiviral transduction

Second generation lentivirus packaging system consisting of psPAX2 (Addgene #12260), pMD2.G (Addgene #12259) and pCMV-GFP as transfection control (Addgene #11153) was used to produce lentivirus particles. After transient transfection in HEK293T cells using polyetylenamine (PEI), lentiviral supernatant was filtered and used to infect target cells using 8 mg/ml polybrene. After infection, the cells were selected with 2 mg/ml puromycin or 10 mg/ml blasticidin. After 48-72h or until non-transduced control cells were dead, the selection was complete.

RNA sequencing and GSEA

Total RNA was extracted with RNeasy mini kit (Qiagen, cat# 74106) including a column DNase digestion (Qiagen, cat#79254), according to the manufacturer's instructions. Quality and quantity of total RNA was assessed by the 2100 Bioanalyzer using a Nano chip (Agilent, Santa Clara, CA). Total RNA samples having RIN>8 were subjected to library generation. Strand-specific libraries were generated using the TruSeq Stranded mRNA samples preparation kit (illumine Inc., San Diego, RS-122-2101/2) according to manufacturer’s instructions (Illumina, part #15031047 Rev.E). Briefly, polyadenylated RNA from intact total RNA was purified using oligo-dT beads. Following purification, the RNA was fragmented, random primed and reverse transcribed using SuperScript II Reverse Transcriptase (Invitrogen, part # 18064-014) with the addition of Actinomycin D. Second strand synthesis was performed using Polymerase I and RNaseH with replacement of dTTP for dUTP. The generated cDNA fragments were 3’ end adenylated and ligated to Illumina Paired-end

684 sequencing adapters and subsequently amplified by 12 cycles of PCR. The libraries were
685 analyzed on a 2100 Bioanalyzer using a 7500 chip (Agilent, Santa Clara, CA), diluted and
686 pooled equimolar into a multiplex sequencing pool. The libraries were sequenced with
687 single-end 65bp reads on a HiSeq 2500 using V4 chemistry (Illumina inc., San Diego).
688 For the analysis, reads were first aligned to a reference genome (hg38) and the datasets
689 were normalized for sequence depth using a relative total size factor. We then performed
690 gene set enrichment analysis (GSEA) using GSEA software[59] with log2FoldChange
691 ranked list as an input. The GSEA preranked tool was used to run the analysis. We used two
692 senescence gene signatures[2,38] as well as gene sets of genes upregulated in
693 senescence from[39,40] to assess enrichment of senescence- associated genes (Table S1).
694
695 In genetic experiments we compared sgCDK2 cells treated with palbociclib with untreated
696 cells and for pharmacological experiments cells treated with palbociclib and indisulam to
697 untreated cells or single treatments. When using PF-0687360 we compared cells treated
698 with the compound to untreated cells. All experiments were performed in duplicates. The *P*-
699 value estimates the statistical significance of the enrichment score and is shown in the
700 figure, unless $P < 0.001$.
701
702 **Splicing error quantification**
703 The RNA was isolated and libraries were prepared as described above. The libraries were
704 sequenced with 75bp paired-end reads on a NextSeq550 using the High Output Kit v2.5,
705 150 Cycles (Illumina Inc., San Diego). For the analysis, sequences were demultiplexed and
706 adapter sequences were trimmed from using SeqPurge[60]. Trimmed reads were aligned to
707 GRCh38 using Hisat2[61] using the prebuilt genome_snp_tran reference. Splice event
708 detection was performed using rMats version 4.0.2 by comparing the replicates of the
709 treated groups to the replicates of the untreated group[62]. rMats events in the different
710 categories were considered significant when the following thresholds were met: having a

711 minimum of 10 reads, an FDR less than 10% and an inclusion-level-difference greater than
712 10%, as described earlier[63].
713
714 **Kinase enrichment analysis**
715 RNa-seq data generated from the splicing experiment was filtered for adjusted p-value <0.05
716 and analysed using the Enrichr software[64] using kinase enrichment analysis[49].
717
718 **CDK2 activity experiments**
719 CDK2 reporter DHB-iRFP was modified from DHB-Venus (Addgene #136461)[46]. Venus
720 was replaced for iRFP713 through Gibson Assembly. In brief, iRFP713 was amplified adding
721 sequence homology and assembled into the BamHI and HpaI sites of the original CDK2
722 reporter plasmid. The following primers were used to amplify iRFP713;
723 F:ACCGATAATCAAGAAACTGGATCCGGGGCCCAGGGCAGCGGCATGGCGGAAGGCTC
724 CGTC R:
725 GTTGATTATCGATAAGCTTGATCCCTCGATGCGGCCGCTTACTCTTCCATCACGCCGAT
726 C.
727 A549 cells were stably transduced with a lentiviral vector containing H2B-GFP (Addgene
728 #25999) and a lentiviral vector containing DHB-iRFP, and subsequently GFP/iRFP double
729 positive cells were isolated by FACS. In order to determine CDK2 activity following 24h drug
730 treatment, cells were seeded in 96 well plate, treated with indisulam and palbociclib for 24h
731 and then imaged on a spinning disc microscope using Andor 505 Dragonfly system
732 equipped with 20x 0.75 NA objective and Zyla 4.2+, sCMOS camera. CDK2 activity was
733 determined by calculating the nucleo/cytoplasmic ratio of the CDK2 reporter, using a custom
734 macro for ImageJ, as described before [65]. For real-time analysis of CDK2 activity
735 immediately following drug treatment, cells were seeded in chambered covered slides
736 (LabtekII), and subsequently imaged for 25h. Inhibitors were added following the first round
737 of image acquisition. Imaging was performed using a Deltavision Elite (Applied Precision)

that was maintained at 5% CO_2 and 37°C, equipped with a 20x 0.75 NA lens (Olympus) and cooled Hamamatsu ORCA R2 Black and White CCD-camera.

Flow cytometry

A549 cells were treated for 24h with indicated doses of palbociclib and indisulam. Cells were then harvested, fixed in ice cold 70% ethanol and stained with DAPI 8 µg/ml in PBS. Samples were acquired with LSRFortessa (BD Biosciences) and analysis was performed with FlowJo10 software. Single cells were gated via DAPI-A and DAPI-H signals and DNA content was gated based on DAPI-A histogram profile.

Western blot

Cells were lysed using RIPA buffer and protein was extracted and quantified using BCA assay (Pierce). Loading buffer and reducing agent (both Thermo Fisher) were added to the samples, which were then boiled for 5 min at 95°C. The samples were resolved on a 5-15% Bis-Tris gel (Thermo Fisher) followed by blotting. Membranes were incubated with primary antibodies diluted to 1:1000 in 5% BSA. Secondary antibodies were used at 1:10000 dilution and were purchased from Biorad. Signal was visualized by the ECL solution (Biorad) using the ChemiDoc Imaging system (Biorad).

Kinase inhibition assay

Inhibition of CDK/cyclin complexes by indisulam was measured by Z'LYTE - SelectScreen Kinase Profiling Services (ThermoFisher). Briefly, CDK/cyclin complexes were incubated with indisulam, substrates and ATP. The kinase activity of the CDK/cyclin complex was measured as ATP consumption, as described in detail previously[45].

Quantitative reverse transcription PCR

RNA was extracted using Isolate II Mini kit (Bioline), following manufacturer's instructions. cDNA was generated using SensiFast cDNA synthesis kit (Bioline) following manufacturer's

766 instructions. For qPCR reaction 1 µg of cDNA was used with SensiFast Sybr Lo-Rox mix
767 (Bioline) and respective primer pair. All reactions were performed in triplicates and the
768 results were analyzed using the deltadelta Ct method. The sequences of primers used are
769 as follows:
770 *RPL13* forward GGCCCAGCAGTACCTGTTTA, *RPL13* reverse AGATGGCGGAGGTGCAG,
771 *RBM39* forward GTCGATGTTAGCTCAGTGCCTC, *RBM39* reverse
772 ACGAAGCATATCTTCAGTTATG, *CCNH* forward TGTTCGGTGTTTAAGCCAGCA, *CCNH*
773 reverse TCCTGGGGTGATATTCCATTACT.
774
775 **Senescence associated B-galactosidase staining**
776 Cells were stained using the Senescence Cells Histochemical Staining kit (CS0030) from
777 Sigma Aldrich according to the manufacturer's instructions. Stained cells were imaged at
778 100x magnification and at least 3 pictures per condition were taken.
779
780 **Colony formation assay and proliferation assay**
781 Cells were plated in 6-well plates with densities between 10-40000 cells per well, depending
782 on the cell line. Medium and drugs were refreshed every 3-4 days. After 10 days the cells
783 were fixed with 4% formaldehyde (Millipore) in PBS, stained with 2% Crystal Violet (Sigma)
784 in water and scanned. For proliferation assays, cells were plated in 96-well plates with
785 densities between 500-2000 cells per well, depending on cell line. Plates were incubated at
786 37°C and images were taken every 4 hours using the IncuCyte ® live cell imaging system.
787 Medium and drugs were refreshed every 3-4 days. Confluency was calculated to generate
788 growth curves.
789
790 **In vivo experiments**
791 All animal experiments were approved by the Animal Ethics Committee of the Netherlands
792 Cancer Institute and were performed in accordance with institutional, national and European

guidelines for Animal Care and Use. CDK2 KO clones used *in vivo* were generated through transient transfection of a plasmid containing Cas9 and gRNA sequences, followed by the brief puromycin selection and characterisation of the clones. For the genetic experiments one million of CAL-51 CDK2 KO single cell clone or control cells in PBS were mixed 1:1 with matrigel and injected orthotopically in the mammary fat pad of 8 weeks female NMRI nude mice (JAX labs), 5-6 mice per group. Furthermore, one million of A549 CDK2 KO single cell clones or control cells in PBS were mixed 1:1 with matrigel and injected subcutaneously in the right flank of NMRI nude mice, 5-6 mice per group. Tumor volume was monitored twice a week and tumor volume was calculated based on the calliper measurements following modified ellipsoidal formula (tumor volume = ½[length x width^2]). For the intervention experiment, one million of A549 cells in PBS were mixed 1:1 with matrigel and injected subcutaneously in the right flank of NMRI nude mice. Upon reaching 200 mm^3, mice were randomized to four treatment groups of 8-12 mice per group: vehicle, indisulam, palbociclib or combination. Palbociclib (dissolved in 50 mM sodium lactate) was administered by oral gavage daily at 100 mg/kg and indisulam (dissolved in 3.5% DMSO, 6.5% Tween 80, 90% saline) by intraperitoneal injection three times per week at 5 mg/kg. Four mice were excluded from the study due to complications of daily intraperitoneal injections (peritonitis).

Immunohistochemistry

Tumors were collected and fixed in EAF fixative (ethanol/acetic acid/formaldehyde/saline at 40:5:10:45 v/v) and embedded in paraffin. For immunohistochemistry, 4 µm-thick sections were made on which antibodies against Ki67 and p21 were applied. The sections were reviewed with a Zeiss Axioskop2 Plus microscope (Carl Zeiss Microscopy) and images were captured with a Zeiss AxioCam HRc digital camera and processed with AxioVision 4 software (both from Carl Zeiss Vision). Histological samples were analyzed by an experienced pathologist. Scoring was performed by quantifying positive area for Ki67 and H-score for p21.

821 **PK/PD experiment for PD and IN**

822 Blood was collected either from the tail vein or by cardiac puncture at different time points
823 indicated in Supplementary Figure 4C and D. Samples were collected on ice using tubes
824 with potassium EDTA as anticoagulant. After cooling, tubes were centrifuged for 10 min
825 5000xg 4°C to separate the plasma fraction, which was then transferred into clean vials and
826 stored at −20°C until analysis. Sample pre-treatment was accomplished by mixing 5µL
827 (plasma) with 60 µL of formic acid in acetonitrile (1+99) containing the internal standard.
828 After centrifugation, the clear supernatant was diluted 1+8 with water and 5µL was injected
829 into the LC-MS/MS system. The samples were assayed twice by liquid chromatography
830 triple quadrupole mass spectrometry (LC-MS/MS) using an API4000 detector (Sciex).
831 Indisulam is detected in negative ionization mode (MRM: 384.2/171.9) and palbociclib in
832 positive ionization mode (MRM: 448.5/320.0). In both cases, LC separation was achieved
833 using a Zorbax Extend C18 column (100 x 2.0 mm: ID). Mobile phase A and B comprised
834 0.1% formic acid in water and methanol, respectively. The flow rate was 0.4ml/min and a
835 linear gradient from 20%B to 95%B in 2.5min, followed by 95%B for 2min, followed by re-
836 equilibration at 20%B for 10min was used for elution.

837

838 **STATISTICAL ANALYSIS**

839 Unpaired t-test and ANOVA were performed with Graphpad Prism (v8.4.3).

840

REFERENCES

1. Ewald JA, Desotelle JA, Wilding G, Jarrard DF. Therapy-induced senescence in cancer. J Natl Cancer Inst. 2010;102: 1536–1546.

2. Fridman AL, Tainsky MA. Critical pathways in cellular senescence and immortalization revealed by gene expression profiling. Oncogene. 2008;27: 5975–5987.

3. Milanovic M, Fan DNY, Belenki D, Däbritz JHM, Zhao Z, Yu Y, et al. Senescence-associated reprogramming promotes cancer stemness. Nature. 2018. pp. 96–100. doi:10.1038/nature25167

4. Wang C, Vegna S, Jin H, Benedict B, Lieftink C, Ramirez C, et al. Inducing and exploiting vulnerabilities for the treatment of liver cancer. Nature. 2019;574: 268–272.

5. Guerrero A, Herranz N, Sun B, Wagner V, Gallage S, Guiho R, et al. Cardiac glycosides are broad-spectrum senolytics. Nat Metab. 2019;1: 1074–1088.

6. Saleh T, Bloukh S, Carpenter VJ, Alwohoush E, Bakeer J, Darwish S, et al. Therapy-Induced Senescence: An “Old” Friend Becomes the Enemy. Cancers . 2020;12: 822.

7. Guan X, LaPak KM, Hennessey RC, Yu CY, Shakya R, Zhang J, et al. Stromal Senescence By Prolonged CDK4/6 Inhibition Potentiates Tumor Growth. Mol Cancer Res. 2017;15: 237–249.

8. Muñoz-Espín D, Rovira M, Galiana I, Giménez C, Lozano-Torres B, Paez-Ribes M, et al. A versatile drug delivery system targeting senescent cells. EMBO Mol Med. 2018;10. doi:10.15252/emmm.201809355

9. Miettinen TP, Peltier J, Härtlova A, Gierliński M, Jansen VM, Trost M, et al. Thermal proteome profiling of breast cancer cells reveals proteasomal activation by CDK4/6 inhibitor palbociclib. EMBO J. 2018;37. doi:10.15252/embj.201798359

10. Torres-Guzmán R, Calsina B, Hermoso A, Baquero C, Alvarez B, Amat J, et al. Preclinical characterization of abemaciclib in hormone receptor positive breast cancer. Oncotarget. 2017;8: 69493–69507.

11. Iyengar M, O’Hayer P, Cole A, Sebastian T, Yang K, Coffman L, et al. CDK4/6 inhibition as maintenance and combination therapy for high grade serous ovarian cancer. Oncotarget. 2018;9: 15658–15672.

12. Malumbres M, Barbacid M. To cycle or not to cycle: a critical decision in cancer. Nat Rev Cancer. 2001;1: 222–231.

13. Sledge GW, Toi M, Neven P, Sohn J, Inoue K, Pivot X, et al. MONARCH 2: Abemaciclib in Combination With Fulvestrant in Women With HR+/HER2− Advanced Breast Cancer Who Had Progressed While Receiving Endocrine Therapy. J Clin Orthod. 2017;35: 2875–2884.

14. Rugo HS, Diéras V, Gelmon KA, Finn RS, Slamon DJ, Martin M, et al. Impact of palbociclib plus letrozole on patient-reported health-related quality of life: results from the PALOMA-2 trial. Ann Oncol. 2018;29: 888–894.

15. Hortobagyi GN, Paluch-Shimon S, Petrakova K, Villanueva C, Chan A, Nusch A, et al. First-line ribociclib (RIB) + letrozole (LET) in hormone receptor-positive (HR+), HER2-negative (HER2–) advanced breast cancer (ABC): MONALEESA-2 biomarker analyses.

J Clin Orthod. 2018;36: 1022–1022.

16. Sherr CJ, Beach D, Shapiro GI. Targeting CDK4 and CDK6: From Discovery to Therapy. Cancer Discov. 2016;6: 353–367.

17. Schettini F, De Santo I, Rea CG, De Placido P, Formisano L, Giuliano M, et al. CDK 4/6 Inhibitors as Single Agent in Advanced Solid Tumors. Front Oncol. 2018;8: 608.

18. Gopalan PK, Pinder MC, Chiappori A, Ivey AM, Villegas AG, Kaye FJ. A phase II clinical trial of the CDK 4/6 inhibitor palbociclib (PD 0332991) in previously treated, advanced non-small cell lung cancer (NSCLC) patients with inactivated CDKN2A. Journal of Clinical Oncology. 2014. pp. 8077–8077. doi:10.1200/jco.2014.32.15_suppl.8077

19. Konecny GE, Wahner Hendrickson AE, Jatoi A, Burton JK, Paroly J, Glaspy JA, et al. A multicenter open-label phase II study of the efficacy and safety of palbociclib a cyclin-dependent kinases 4 and 6 inhibitor in patients with recurrent ovarian cancer. J Clin Orthod. 2016;34: 5557–5557.

20. Turner NC, Liu Y, Zhu Z, Loi S, Colleoni M, Loibl S, et al. Cyclin E1 Expression and Palbociclib Efficacy in Previously Treated Hormone Receptor-Positive Metastatic Breast Cancer. J Clin Oncol. 2019;37: 1169–1178.

21. Morris-Hanon O, Marazita MC, Romorini L, Isaja L, Fernandez-Espinosa DD, Sevlever GE, et al. Palbociclib Effectively Halts Proliferation but Fails to Induce Senescence in Patient-Derived Glioma Stem Cells. Mol Neurobiol. 2019;56: 7810–7821.

22. Fassl A, Brain C, Abu-Remaileh M, Stukan I, Butter D, Stepien P, et al. Increased lysosomal biomass is responsible for the resistance of triple-negative breast cancers to CDK4/6 inhibition. Sci Adv. 2020;6: eabb2210.

23. Haines E, Chen T, Kommajosyula N, Chen Z, Herter-Sprie GS, Cornell L, et al. Palbociclib resistance confers dependence on an FGFR-MAP kinase-mTOR-driven pathway in KRAS-mutant non-small cell lung cancer. Oncotarget. 2018;9: 31572–31589.

24. Herrera-Abreu MT, Palafox M, Asghar U, Rivas MA. Early adaptation and acquired resistance to CDK4/6 inhibition in estrogen receptor–positive breast cancer. Cancer Res. 2016. Available: http://cancerres.aacrjournals.org/content/76/8/2301.short

25. Vora SR, Juric D, Kim N, Mino-Kenudson M, Huynh T, Costa C, et al. CDK 4/6 inhibitors sensitize PIK3CA mutant breast cancer to PI3K inhibitors. Cancer Cell. 2014;26: 136–149.

26. Ruscetti M, Leibold J, Bott MJ, Fennell M. NK cell–mediated cytotoxicity contributes to tumor control by a cytostatic drug combination. 2018. Available: https://science.sciencemag.org/content/362/6421/1416.abstract?casa_token=xqbhMa9rLysAAAAA:IicKqq8A-eetp0IF500MdGNsn5Sru5wY1fplLa9ZFxJM_5iDyOXKOSmmRNv9zk6_mnnG_xLDzdZNNqU

27. Lee MS, Helms TL, Feng N, Gay J, Chang QE, Tian F, et al. Efficacy of the combination of MEK and CDK4/6 inhibitors in vitro and in vivo in KRAS mutant colorectal cancer models. Oncotarget. 2016;7: 39595–39608.

28. Haddad RI, Weinstein LJ, Wieczorek TJ, Bhattacharya N, Raftopoulos H, Oster MW, et al. A phase II clinical and pharmacodynamic study of E7070 in patients with metastatic,

recurrent, or refractory squamous cell carcinoma of the head and neck: modulation of retinoblastoma protein phosphorylation by a novel chloroindolyl sulfonamide cell cycle inhibitor. Clin Cancer Res. 2004;10: 4680–4687.

29. Smyth JF, Aamdal S, Awada A, Dittrich C, Caponigro F, Schöffski P, et al. Phase II study of E7070 in patients with metastatic melanoma. Ann Oncol. 2005;16: 158–161.

30. Talbot DC, von Pawel J, Cattell E, Murray Yule S, Johnston C, Zandvliet AS, et al. A Randomized Phase II Pharmacokinetic and Pharmacodynamic Study of Indisulam as Second-Line Therapy in Patients with Advanced Non–Small Cell Lung Cancer. Clin Cancer Res. 2007;13: 1816–1822.

31. Punt CJA, Fumoleau P, van de Walle B, Faber MN, Ravic M, Campone M. Phase I and pharmacokinetic study of E7070, a novel sulfonamide, given at a daily times five schedule in patients with solid tumors. A study by the EORTC-Early Clinical Studies Group (ECSG). Annals of Oncology. 2001. pp. 1289–1293. doi:10.1023/a:1012287111922

32. Raymond E, ten Bokkel Huinink WW, Taïeb J, Beijnen JH, Faivre S, Wanders J, et al. Phase I and pharmacokinetic study of E7070, a novel chloroindolyl sulfonamide cell-cycle inhibitor, administered as a one-hour infusion every three weeks in patients with advanced cancer. J Clin Oncol. 2002;20: 3508–3521.

33. Dittrich C, Dumez H, Calvert H, Hanauske A, Faber M, Wanders J, et al. Phase I and pharmacokinetic study of E7070, a chloroindolyl-sulfonamide anticancer agent, administered on a weekly schedule to patients with solid tumors. Clin Cancer Res. 2003;9: 5195–5204.

34. Yamada Y, Yamamoto N, Shimoyama T, Horiike A, Fujisaka Y, Takayama K, et al. Phase I pharmacokinetic and pharmacogenomic study of E7070 administered once every 21 days. Cancer Sci. 2005;96: 721–728.

35. Han T, Goralski M, Gaskill N, Capota E, Kim J, Ting TC, et al. Anticancer sulfonamides target splicing by inducing RBM39 degradation via recruitment to DCAF15. Science. 2017;356. doi:10.1126/science.aal3755

36. Prahallad A, Sun C, Huang S, Di Nicolantonio F, Salazar R, Zecchin D, et al. Unresponsiveness of colon cancer to BRAF(V600E) inhibition through feedback activation of EGFR. Nature. 2012;483: 100–103.

37. Gorgoulis V, Adams PD, Alimonti A, Bennett DC, Bischof O, Bishop C, et al. Cellular Senescence: Defining a Path Forward. Cell. 2019;179: 813–827.

38. Casella G, Munk R, Kim KM, Piao Y, De S, Abdelmohsen K, et al. Transcriptome signature of cellular senescence. Nucleic Acids Res. 2019;47: 11476.

39. Purcell M, Kruger A, Tainsky MA. Gene expression profiling of replicative and induced senescence. Cell Cycle. 2014;13: 3927–3937.

40. Hernandez-Segura A, de Jong TV, Melov S, Guryev V, Campisi J, Demaria M. Unmasking Transcriptional Heterogeneity in Senescent Cells. Curr Biol. 2017;27: 2652–2660.e4.

41. Tadesse S, Anshabo AT, Portman N, Lim E, Tilley W, Caldon CE, et al. Targeting CDK2 in cancer: challenges and opportunities for therapy. Drug Discov Today. 2020;25: 406–413.

42. Fukuoka K, Usuda J, Iwamoto Y, Fukumoto H, Nakamura T, Yoneda T, et al. Mechanisms of action of the novel sulfonamide anticancer agent E7070 on cell cycle progression in human non-small cell lung cancer cells. Invest New Drugs. 2001;19: 219–227.

43. Kumarasamy V, Vail P, Nambiar R, Witkiewicz AK, Knudsen ES. Functional Determinants of Cell Cycle Plasticity and Sensitivity to CDK4/6 Inhibition. Cancer Res. 2021;81: 1347–1360.

44. Freeman-Cook K, Hoffman RL, Miller N, Almaden J, Chionis J, Zhang Q, et al. Expanding control of the tumor cell cycle with a CDK2/4/6 inhibitor. Cancer Cell. 2021;39: 1404–1421.e11.

45. Hafner M, Mills CE, Subramanian K, Chen C, Chung M, Boswell SA, et al. Multiomics Profiling Establishes the Polypharmacology of FDA-Approved CDK4/6 Inhibitors and the Potential for Differential Clinical Activity. Cell Chem Biol. 2019;26: 1067–1080.e8.

46. Spencer SL, Cappell SD, Tsai F-C, Overton KW, Wang CL, Meyer T. The proliferation-quiescence decision is controlled by a bifurcation in CDK2 activity at mitotic exit. Cell. 2013;155: 369–383.

47. Welcker M, Singer J, Loeb KR, Grim J, Bloecher A, Gurien-West M, et al. Multisite phosphorylation by Cdk2 and GSK3 controls cyclin E degradation. Mol Cell. 2003;12: 381–392.

48. Clurman BE, Sheaff RJ, Thress K, Groudine M, Roberts JM. Turnover of cyclin E by the ubiquitin-proteasome pathway is regulated by cdk2 binding and cyclin phosphorylation. Genes Dev. 1996;10: 1979–1990.

49. Lachmann A, Ma'ayan A. KEA: kinase enrichment analysis. Bioinformatics. 2009;25: 684–686.

50. Finn RS, Dering J, Conklin D, Kalous O, Cohen DJ, Desai AJ, et al. PD 0332991, a selective cyclin D kinase 4/6 inhibitor, preferentially inhibits proliferation of luminal estrogen receptor-positive human breast cancer cell lines in vitro. Breast Cancer Research. 2009. doi:10.1186/bcr2419

51. Mulero-Sánchez A, Pogacar Z, Vecchione L. Importance of genetic screens in precision oncology. ESMO Open. 2019;4: e000505.

52. Gong X, Litchfield LM, Webster Y, Chio L-C, Wong SS, Stewart TR, et al. Genomic Aberrations that Activate D-type Cyclins Are Associated with Enhanced Sensitivity to the CDK4 and CDK6 Inhibitor Abemaciclib. Cancer Cell. 2017;32: 761–776.e6.

53. Pandey K, Park N, Park K-S, Hur J, Cho YB, Kang M, et al. Combined CDK2 and CDK4/6 Inhibition Overcomes Palbociclib Resistance in Breast Cancer by Enhancing Senescence. Cancers . 2020;12. doi:10.3390/cancers12123566

54. Simoneschi D, Rona G, Zhou N, Jeong Y-T, Jiang S, Milletti G, et al. CRL4AMBRA1 is a master regulator of D-type cyclins. Nature. 2021. doi:10.1038/s41586-021-03445-y

55. Ruscetti M, Morris JP 4th, Mezzadra R, Russell J, Leibold J, Romesser PB, et al. Senescence-Induced Vascular Remodeling Creates Therapeutic Vulnerabilities in Pancreas Cancer. Cell. 2020;181: 424–441.e21.

56. Love MI, Huber W, Anders S. Moderated estimation of fold change and dispersion for

RNA-seq data with DESeq2. Genome Biol. 2014;15: 550.

57. Evers B, Jastrzebski K, Heijmans JPM, Grernrum W, Beijersbergen RL, Bernards R. CRISPR knockout screening outperforms shRNA and CRISPRi in identifying essential genes. Nat Biotechnol. 2016;34: 631–633.

58. Beijersbergen RL, Carlée L, Kerkhoven RM, Bernards R. Regulation of the retinoblastoma protein-related p107 by G1 cyclin complexes. Genes Dev. 1995;9: 1340–1353.

59. Subramanian A, Tamayo P, Mootha VK, Mukherjee S, Ebert BL, Gillette MA, et al. Gene set enrichment analysis: a knowledge-based approach for interpreting genome-wide expression profiles. Proc Natl Acad Sci U S A. 2005;102: 15545–15550.

60. Sturm M, Schroeder C, Bauer P. SeqPurge: highly-sensitive adapter trimming for paired-end NGS data. BMC Bioinformatics. 2016;17: 208.

61. Kim D, Paggi JM, Park C, Bennett C, Salzberg SL. Graph-based genome alignment and genotyping with HISAT2 and HISAT-genotype. Nat Biotechnol. 2019;37: 907–915.

62. Shen S, Park JW, Lu Z-X, Lin L, Henry MD, Wu YN, et al. rMATS: robust and flexible detection of differential alternative splicing from replicate RNA-Seq data. Proc Natl Acad Sci U S A. 2014;111: E5593–601.

63. Wang E, Lu SX, Pastore A, Chen X, Imig J, Chun-Wei Lee S, et al. Targeting an RNA-Binding Protein Network in Acute Myeloid Leukemia. Cancer Cell. 2019;35: 369–384.e7.

64. Chen EY, Tan CM, Kou Y, Duan Q, Wang Z, Meirelles GV, et al. Enrichr: interactive and collaborative HTML5 gene list enrichment analysis tool. BMC Bioinformatics. 2013;14: 128.

65. Menegakis A, Klompmaker R, Vennin C, Arbusà A, Damen M, van den Broek B, et al. Resistance of Hypoxic Cells to Ionizing Radiation Is Mediated in Part via Hypoxia-Induced Quiescence. Cells. 2021;10. doi:10.3390/cells10030610

Figure 1

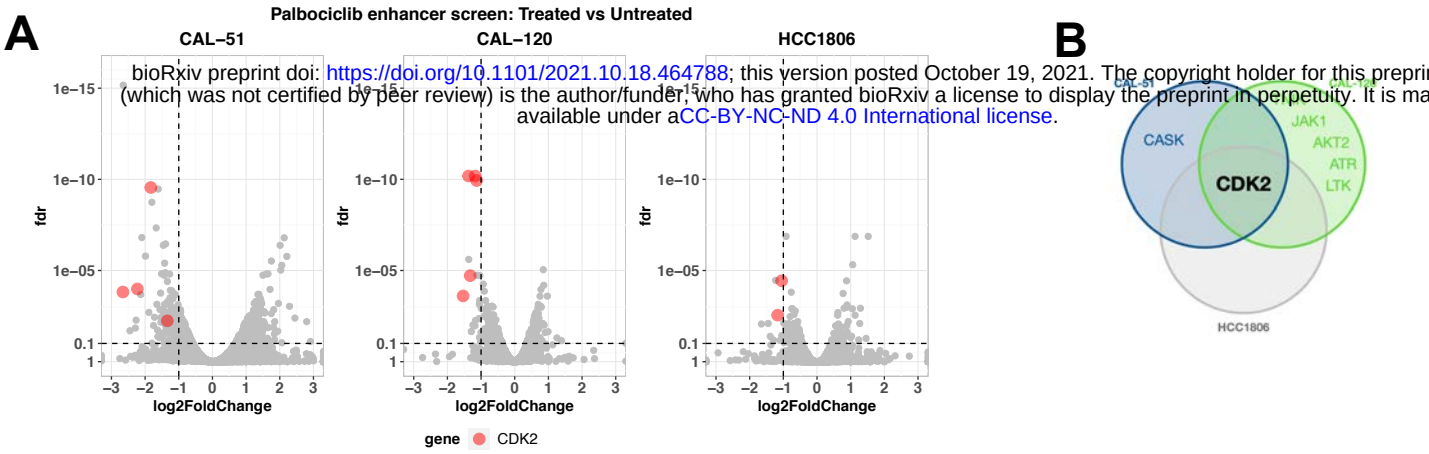

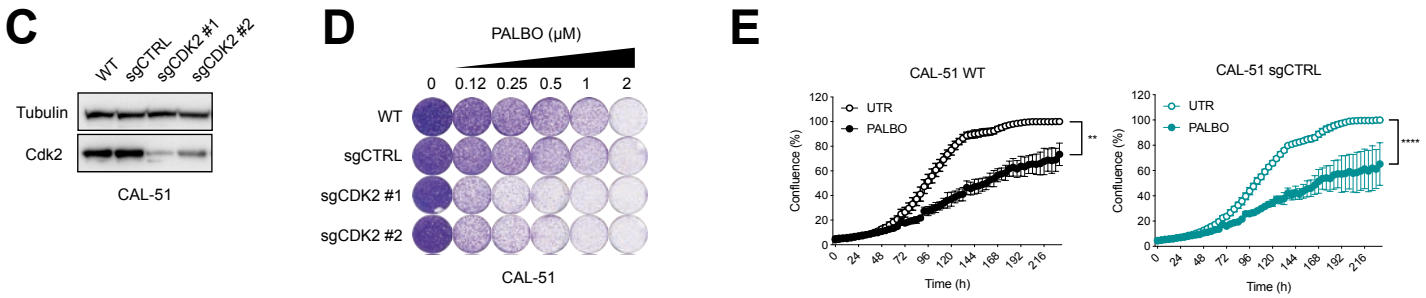

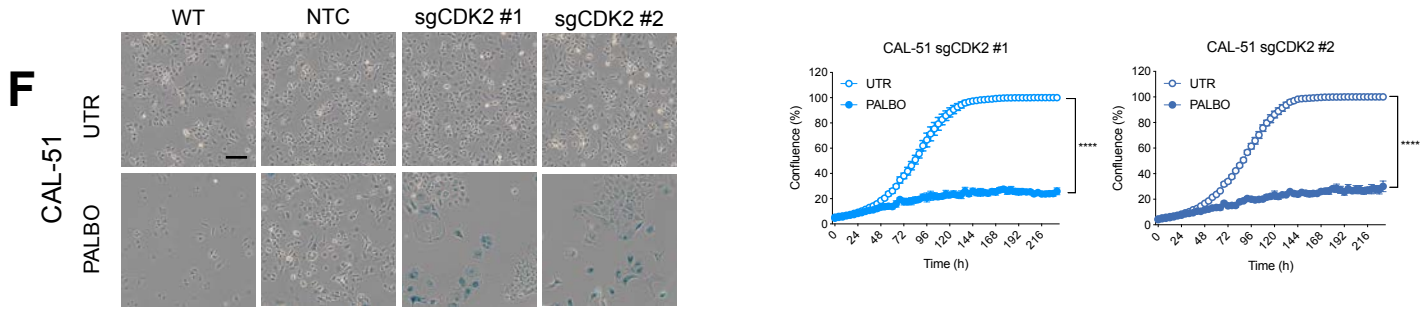

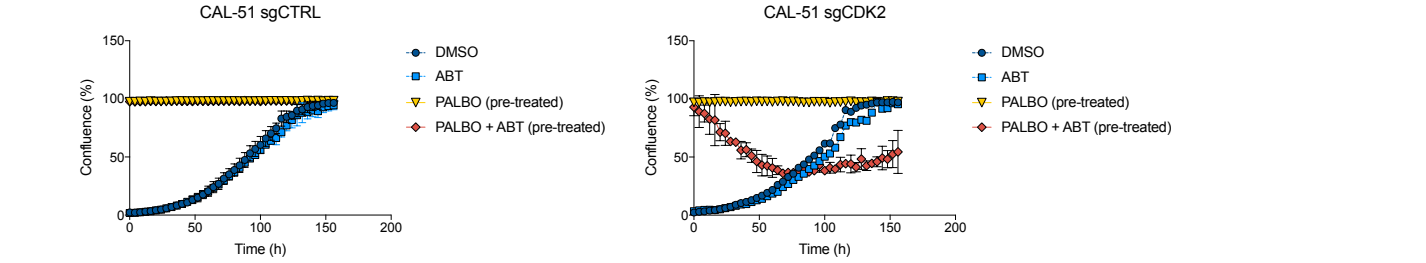

Figure 2

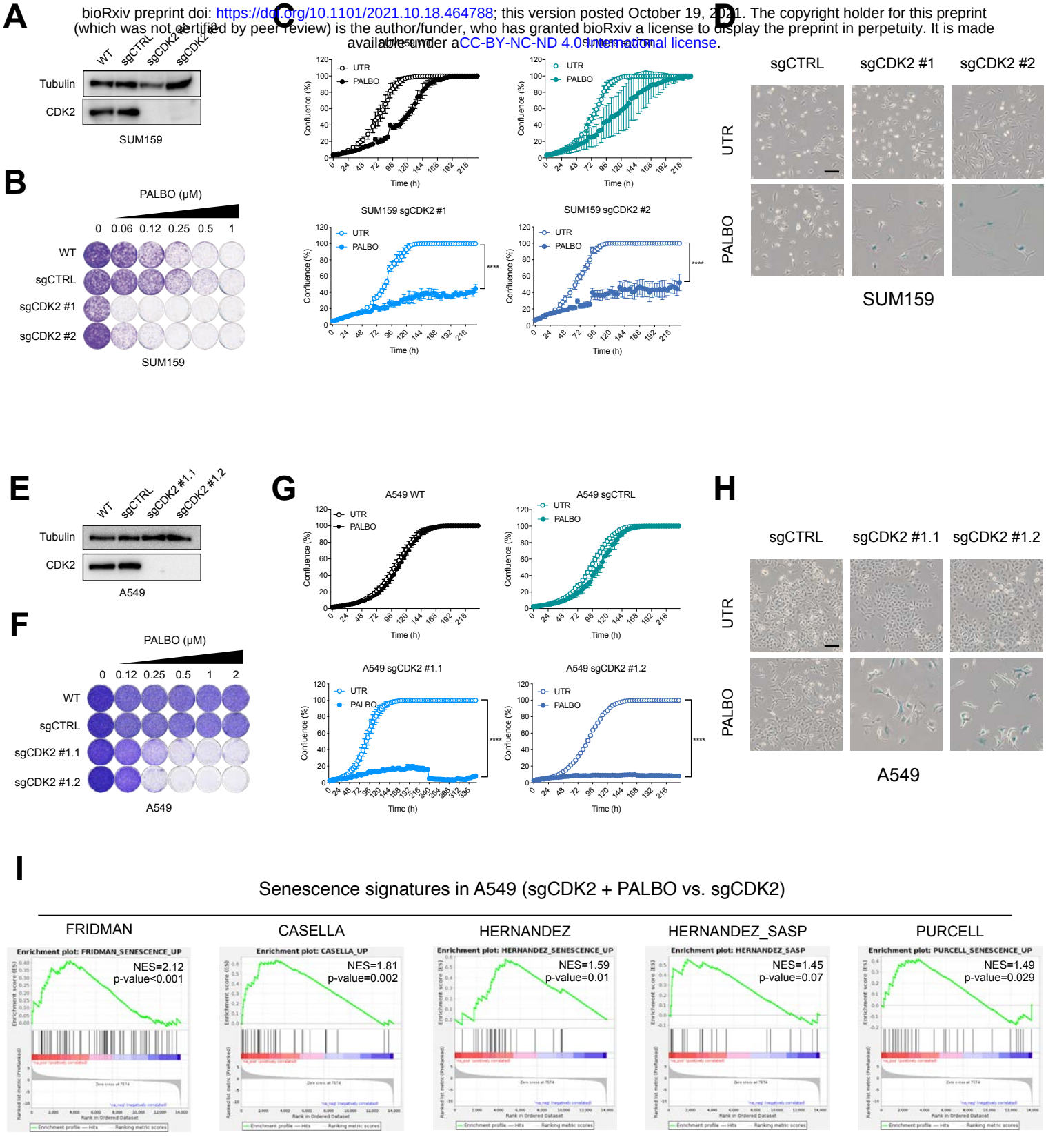

Figure 3

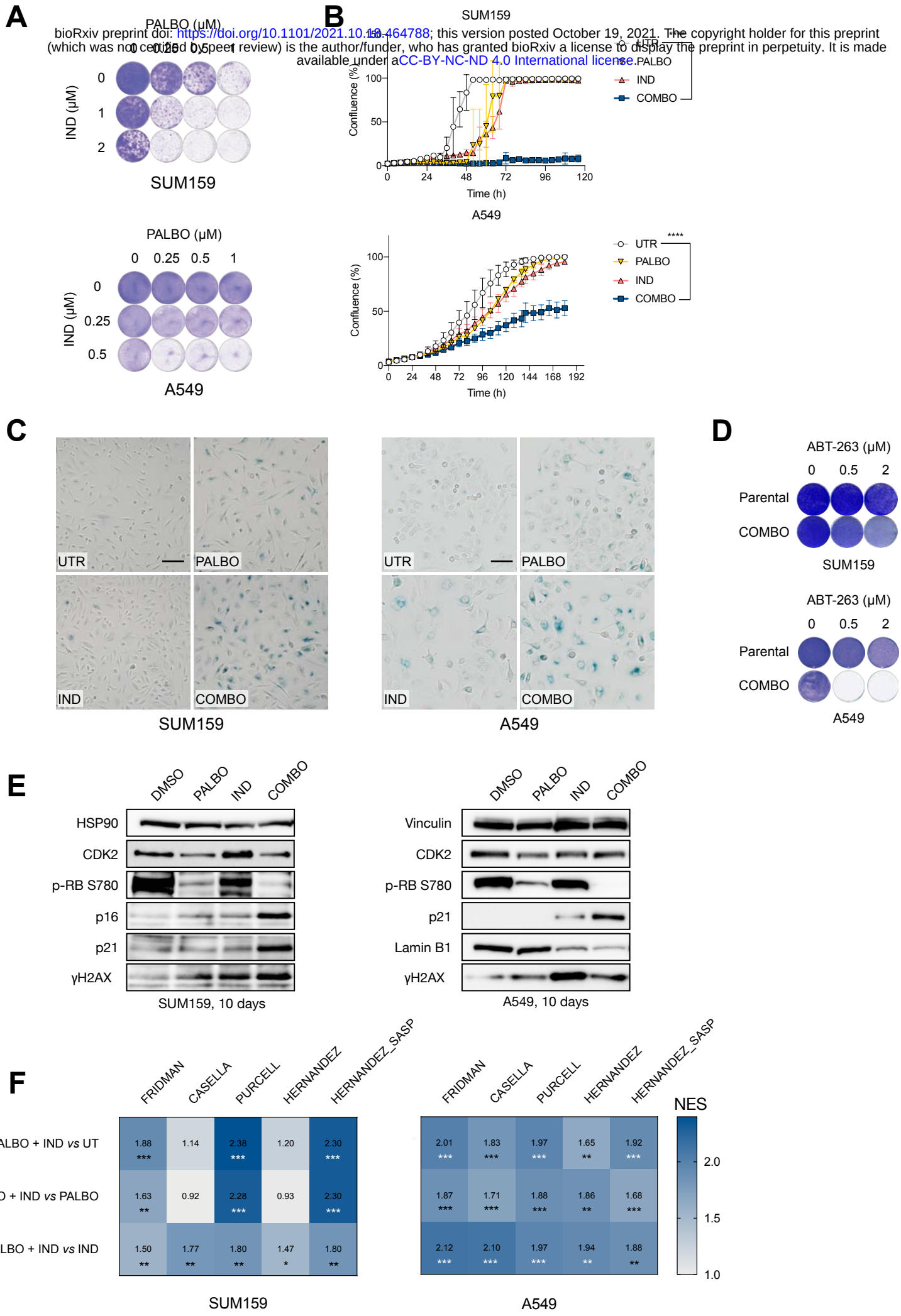

Figure 4

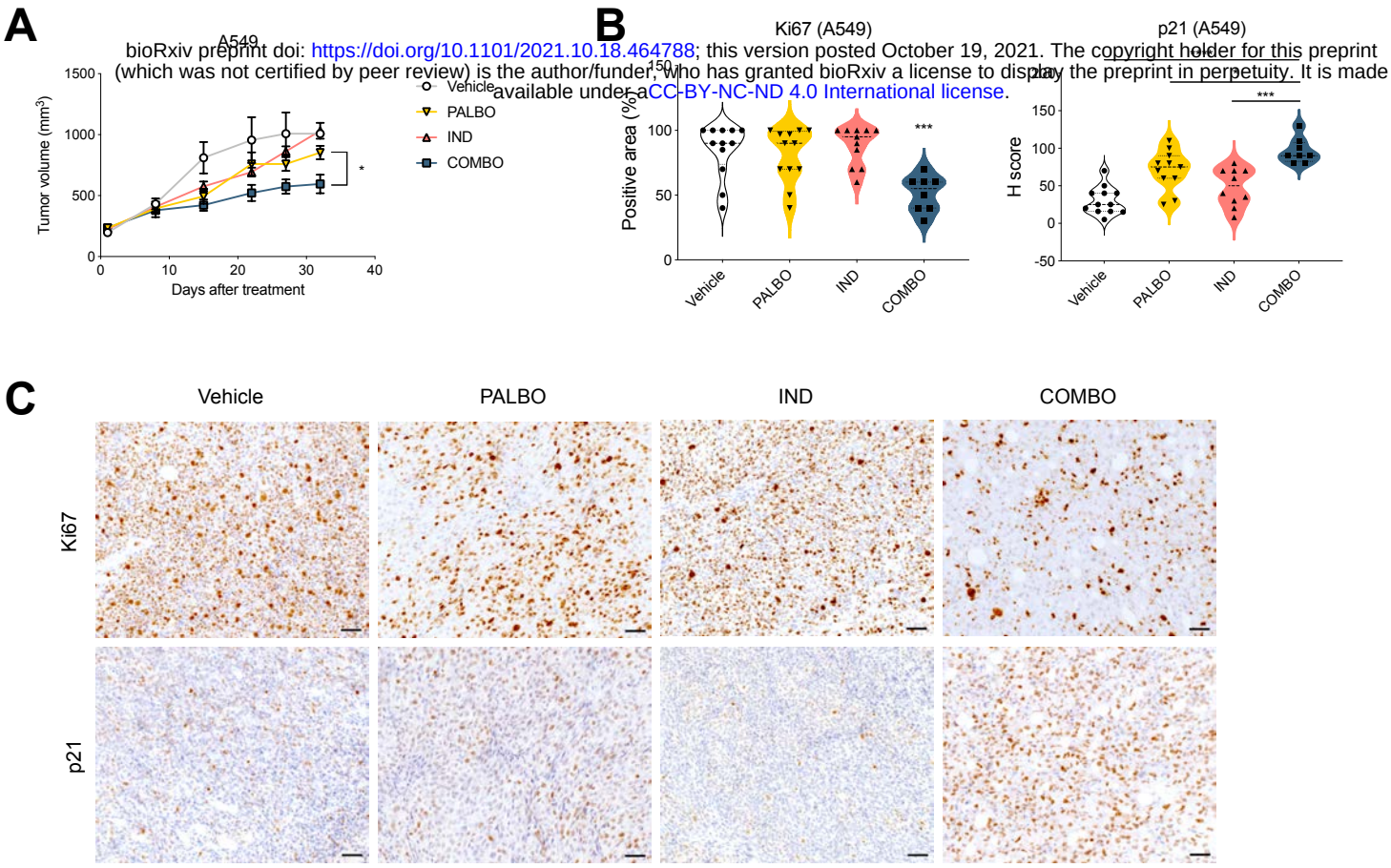

Figure 5